

# Magnetically enhanced gliding arc discharge for CO<sub>2</sub> activation

Li Li<sup>a</sup>, Hao Zhang<sup>a,\*</sup>, Xiaodong Li<sup>a</sup>, Jingying Huang<sup>a</sup>, Xiangzhi Kong<sup>a</sup>, Ruiyang Xu<sup>a</sup>, Xin Tu<sup>b,\*</sup>

<sup>a</sup> State Key Laboratory of Clean Energy Utilization, Zhejiang University, Hangzhou 310027, China

<sup>b</sup> Department of Electrical Engineering and Electronics, University of Liverpool, Liverpool L69 3GJ, UK

## Abstract:

In this work, a novel magnetically enhanced gliding arc discharge (MEGAD) reactor was developed and investigated for the activation of carbon dioxide to produce value-added carbon monoxide. The effect of the external magnetic field on the gliding arc motion behavior, electrical characteristics and CO<sub>2</sub> decomposition has been systematically investigated under different flow rates. Results indicate that the presence of the external magnetic field can remarkably enlarge the plasma region, due to the facilitating effect of Lorentz force, especially at a low flow rate. The gliding arc motions with and without a magnetic field at low flow rates show different patterns: a short-circuiting pattern of a “motionless” gliding arc without a magnetic field and a regular ‘ignition – elongation – extinguishment’ pattern of a motional gliding arc with a magnetic field. Interestingly, the MEGAD exhibits higher CO<sub>2</sub> conversion in comparison to traditional gliding arc systems (up to 40.6% higher at flow rate = 1 L/min), especially at relatively low flow rates. The optimal CO<sub>2</sub> dissociation performance achieved is: 12.2% CO<sub>2</sub> conversion and 24.3% energy efficiency at 3000 mL/min or 11.2% CO<sub>2</sub> conversion and 27.9% energy efficiency at 4000 mL/min, with the presence of magnetic field.

**Keywords:** CO<sub>2</sub> decomposition, gliding arc discharge, magnetic field, flow rate, motion behavior

## 1 Introduction

With the rapid development of industry and increasing depletion of fossil fuels, the emission of anthropogenic carbon dioxide, which is the major greenhouse gas, has reached the highest level on record (up to  $37.1 \pm 1.8$  Gt CO<sub>2</sub> in 2018) [1]. It is evidenced that increasing atmospheric CO<sub>2</sub> concentration leads to climate change [2]. Undoubtedly, the development of effective strategies for CO<sub>2</sub> emission control has been of urgent importance.

Currently, increasing studies on CO<sub>2</sub> treatment are involved to carbon capture, utilization and

---

\* Corresponding authors. Tel.: +86 571 87952037 (H. Zhang), +44 1517944513 (X. Tu).  
E-mail addresses: [zhang\\_hao@zju.edu.cn](mailto:zhang_hao@zju.edu.cn) (H. Zhang), [xin.tu@liverpool.ac.uk](mailto:xin.tu@liverpool.ac.uk) (X. Tu)

1 storage (CCUS) [3][4]. Direct decomposition of CO<sub>2</sub> has attracted particular interest as one of the  
2 CCUS routes, because it can recycle CO<sub>2</sub> into value-added CO, which can serve not only as a kind of  
3 fuel but also a widely used chemical feedstock [5]. However, the CO<sub>2</sub> molecule is too stable to be  
4 activated and it needs up to 523 kJ/mol energy to destroy the C=O chemical bonds [6]. In traditional  
5 thermal splitting route, a high temperature of up to 1954 K can provide a CO<sub>2</sub> conversion of only 1.2%  
6 CO<sub>2</sub> [7], which is obviously energy consuming and industrially unfavorable. In this regard,  
7 atmospheric non-thermal plasma technology is emerging as a promising alternative [8]. Plasma is a  
8 highly active system full of reactive species like energetic electrons, radicals, excited species, ions and  
9 atoms etc. Typically, plasma can be classified into thermal and non-thermal plasmas. Thermal plasma  
10 is more powerful but the gas temperature is as high as that of electrons (e.g., > 10<sup>4</sup> K) and normally  
11 leads to high energy consumption. In non-thermal plasmas, the average electron temperature can be as  
12 high as 1–10 eV [9], while the heavy particle temperature (gas temperature) can remain fairly low (e.g.,  
13 < 800°C or even room temperature), ensuring a lower heat loss [10][11][12]. The energetic electrons  
14 are considered as the initiators of the plasma chemical reactions and it can allow the “activation” of  
15 the stable CO<sub>2</sub> molecules even at atmospheric pressure [13]. Therefore, non-thermal plasma is  
16 attracting increasing attention for CO<sub>2</sub> activation in recent years [14]. Among different kinds of non-  
17 thermal plasma sources, gliding arc discharge (GAD) is being spotlighted because it shows the merits  
18 of both non-thermal and thermal plasmas [12][15]. The electron temperature of GAD is typically 1-2  
19 eV, which is most suitable for the efficient vibrational excitation of CO<sub>2</sub> [13][16][17]. It has been  
20 evidenced that the vibrational excitation dissociation is the most effective CO<sub>2</sub> dissociation route [18].  
21 Traditionally, an atmospheric-pressure GAD contains two semi-ellipsoidal steel electrodes, and the  
22 high-voltage power supply initiates electrical breakdown at the shortest gap between the two electrodes,  
23 then the gas flow in between the electrodes push the gliding arc moving along the electrodes. The  
24 gliding arc is elongated during this process and requires more power from power supply to sustain  
25 itself [19][20]. When the length of the gliding arc reaches a critical value  $l_{crit}$ , the power supply is  
26 unable to provide sufficient energy to balance the heat losses from the plasma column. The gliding arc  
27 then cools down rapidly in this stage, which is called *non-equilibrium stage* [15]. The critical length  
28  $l_{crit}$  of gliding arc plays an important role in reaction, as a longer critical length  $l_{crit}$  indicates a larger  
29 plasma region, which leads to a longer retention time of the reactant gas in the plasma area.

1 Normally, a high flow rates of 10-20 L/min is indispensable to enable the gliding arc moving  
2 along the electrodes and sustaining an effective plasma area. Whereas, this results in a low  $l_{crit}$  due to  
3 the significant heat loss, leading to a limited plasma area for chemical reaction, which is undoubtedly  
4 detrimental to the treatment of gas and the conversion efficiency [10][21]. To solve this problem,  
5 several efforts have been devoted to improve the reactors, such as the developed rotating gliding arc  
6 (RGA) [19][20][22][23], in which ring magnets were used to stabilize the gliding arc. A relatively long  
7 and stable rotating arc can be formed in the RGA with the help of a magnetic field (or co-driven by  
8 magnetic field and tangential gas flow), generating a nearly 3D large plasma region. However, the  
9 gliding arc of RGA typically sustains in the *near-equilibrium stage* and exhibits a high gas temperature  
10 (e.g., 800°C), while such a high gas temperature is proved to be unfavorable for CO<sub>2</sub> decomposition  
11 [8][24].

12 In this work, a novel magnetically enhanced gliding arc discharge (MEGAD) reactor is developed  
13 for CO<sub>2</sub> activation. Compared with traditional GAD that driven by gas flow, the magnetic field in the  
14 MEGAD can provide an extra Lorentz force for the moving gliding arc. A synergistic effect of gas  
15 flow and Lorentz force can powerfully push the gliding arc motion along the electrodes and increase  
16 the critical length  $l_{crit}$ . In this way, a larger plasma area can be formed for chemical reaction. Although  
17 similar idea of integrating a magnetic field into a traditional gliding arc has been reported [25][26], no  
18 detailed investigation was performed. In addition, unlike the commonly used cylindrical covers in  
19 almost all of the reported works [27][28][29], a cuboid quartz cover is innovatively designed in this  
20 work to increase the fraction of CO<sub>2</sub> treated. In this study, the physical characteristics of this novel  
21 MEGAD reactor are systematically investigated including the gliding arc motion behavior and  
22 electrical characteristics. It is then investigated for CO<sub>2</sub> decomposition with specific focus on the effect  
23 of the addition of magnetic field on the reaction performance under varying flow rates.

## 24 25 26 **2 Experimental**

### 27 **2.1 Experimental setup**

28

29 Fig. 1. Schematic diagram of the experimental setup.  
30

Figure 1 shows the schematic diagram of the experimental setup. The MEGAD reactor consists of two knife-shaped electrodes (with a length of 17 mm and base width of 2 mm), a gas nozzle with inner diameter of 1.0 mm, a quadrangular quartz cover with dimension of 45×11×120 mm. Two flat magnets were placed on both sides of the quartz cover, producing a uniform magnetic field in the direction of perpendicular to the quartz cover. A thermocouple thermometer (TM-902C+ WRNK-81530) is placed 80 mm downstream end of the electrode assembly to measure the temperature of the outlet gas. A DC power supply (Teslaman TLP2040, 10 kV) is connected to one of the electrodes while the other is grounded. A 40-kΩ resistance is connected in a series circuit to limit and stabilize the discharge current. The voltage and the current of discharge are measured by an oscilloscope (Tektronix DPO4030B) equipped with a high-voltage probe (Tektronix P6015A) and discharge current probe (Tektronix TCP303). The motion behavior of discharge gliding arc is recorded by a high-performance high-speed camera (Phantom V2512). The flow rate of CO<sub>2</sub> (purity, 99.99%) is controlled by a mass flow controller (MFC, YJ-700C). The CO<sub>2</sub> concentration of effluent gas is detected by a portable CO<sub>2</sub> analyzer (GXH-3010E1, Huayun Instrument), using Non-Dispersive Infrared (NDIR) to quantify gases. Meanwhile, samples are collected to analyze the production by using a gas chromatograph (GC, GC9790A, Fuli Analytical Instrument Co.) which is equipped with a flame ionization detector (FID) with a catalytic methanation unit for detecting CO and a thermal conductivity detector (TCD) for the measurement of O<sub>2</sub>. The surfaces of electrodes are analyzed by a metalloscope (Axio Scope A1).

## 2.2 Reaction performance parameters

The parameters to evaluate the performance of the system are defined as follow:

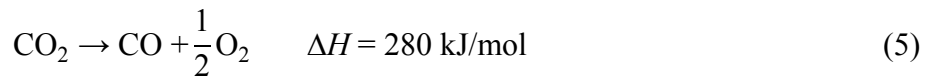
$$X_{CO_2}(\%) = \frac{Q_{CO_2}(\text{mol/s}) - Q'(\text{mol/s}) \times C_{CO_2}(\%)}{Q_{CO_2}(\text{mol/s})} \times 100\% \quad (1)$$

$$B_{Carbon}(\%) = \frac{Q'(\text{mol/s}) \times C_{CO}(\%) + Q'(\text{mol/s}) \times C_{CO_2}(\%)}{Q_{CO_2}(\text{mol/s})} \times 100\% \quad (2)$$

$$\eta(\%) = \frac{X_{CO_2}(\%) \times Q_{CO_2}(\text{mol/s}) \times \Delta H(\text{J/mol})}{\text{Discharge power (W)}} \times 100\% \quad (3)$$

$$SEI \text{ (kJ/L)} = \frac{\text{Discharge power (W)}}{\text{CO}_2 \text{ flow rate (mL/s)}} \quad (4)$$

Where,  $X_{CO_2}$  is  $CO_2$  conversion;  $Q_{CO_2}$  and  $Q'$  are the inlet  $CO_2$  flow rate and outlet total flow rate, respectively;  $C_{CO_2}$  is the  $CO_2$  concentration in the outlet effluent gas;  $B_{Carbon}$  is carbon balance;  $\eta$  is energy efficiency;  $\Delta H$  is the standard reaction enthalpy of eq. (5);  $SEI$  is specific energy input, which is used to evaluate the energy density.



The carbon balance under the studied conditions is ranging between 95.0 % to 99.6 %, and no observable carbon deposition formed in the reactor. Considering the systematical errors and random errors, the major reaction can be assumed as the decomposition of  $CO_2$  into  $CO$  and  $O_2$ . Therefore, the  $CO_2$  conversion and energy efficiency can be considered as the main indicators of the reaction performance.

### 3 Results and discussion

#### 3.1 Gliding arc motion and electrical characteristics

To record the gliding arc motion in magnetic field using a high-speed camera, only one flat magnet is used in this section to enable the gliding arc to be visible from one side. Three typical conditions are investigated to evaluate the effect of the magnetic field: (1) without flow (0 L/min, pre-filled with  $CO_2$ ); (2) low flow rate (2 L/min); (3) high flow rate (8 L/min). The high-speed camera was operated at 39,000 frames per second and equipped with a Nikon lens ( $f = 50 \text{ mm}$ , aperture =  $f/5.6$ ). In addition, the cathode connected to the ground is situated at the right side of all pictures.

Figure 2 represents the photographs of the GAD plasma without/with magnetic field under condition of (1) without flow (0 L/min). Obviously, the addition of magnetic field significantly influenced the discharge. In the GAD without magnetic field, a highly bright and stable short arc is maintained at the narrowest gap between the electrodes without moving downwards (see Fig. 2a).

1 While in the MEGAD with a magnetic field, the gliding arc can generate a huge visible blurred glowing  
2 region (see Fig. 2b), and the plasma region stretches across the cross-section of the cover with a length  
3 of up to 70 mm. With the existence of the external magnetic field, a force perpendicular to the direction  
4 of the arc can be formed on the gliding arc, as schematically shown in Fig. 3, pushing the arc moving  
5 along the electrodes even without gas flow. Traditionally, a gliding arc discharge needs a relatively  
6 high gas flow rate (e.g., 10-20 L/min) to enable the gliding arc moving along the electrodes, forming  
7 an effective plasma region. However, the MEGAD can form a significant plasma area for reaction even  
8 without gas injected. The unique property of the MEGAD could be of significant benefit not only for  
9 the improvement of reaction performance but also for practical applications of GAD.

10 Figure 4a depicts the electrical characteristics of both with/without magnetic field under condition  
11 of (1) without flow (0 L/min). The high-speed frames of the gliding arc motion behavior without and  
12 with magnetic field are illustrated in Fig. 4b and Fig. 4c respectively. The time interval between each  
13 gliding arc is 3 ms (exposure time = 25.2  $\mu$ s). Under conditions of both without and with magnetic  
14 field in Fig. 4b and Fig. 4c, a new ignition is generated at the narrowest gap between two electrodes at  
15  $t_1$ , and the gliding arc connects the anchor points on the electrodes and the discharge current passes  
16 through the gliding arc. Obviously, no further movement of the gliding arc (from  $t_1$  to  $t_3$ ) in the GAD  
17 without magnetic field can be observed in Fig. 4b and the discharge voltage and current both remain  
18 nearly constant. However, for the MEGAD with magnetic field, a tremendous drop takes place in both  
19 the voltage (from 2,460 to 340 V) and the current (from 209.2 to 236.4 mA) at  $t_1$ . Afterwards, the  
20 gliding arc motion is accelerated by the Lorentz force along the electrodes and gradually elongated  
21 (from  $t_1$  to  $t_3$ ), which leads to an increase of its resistance (from approximately 1,500 to 12,000  $\Omega$ ).  
22 Hence, the voltage increases and the current decreases continuously. At  $t_3$ , the length of gliding arc  
23 reaches the critical value  $l_{crit}$ , which is usually determined by the power supply limits [15][30].  
24 Therefore, the gliding arc extinguishes when the heat losses exceed the energy supplied by the source.  
25 A new ignition generates at the same time at the narrowest gap and the next cycle starts while the  
26 emission of last plasma column is still visible. The visible emissions decay with a short time of  
27 approximately 1 ms (see Fig. 5). The phenomenon of visible emissions of former plasma column is  
28 also reported in a study by Sun et al. [31]. The gliding arc motion with magnetic field shows a stable  
29 period of about 22 ms.

1  
2  
3  
4  
5  
6  
7  
8  
9  
10  
11  
12  
13  
14  
15  
16  
17  
18  
19  
20  
21  
22  
23  
24  
25  
26  
27  
28  
29

Fig. 2. Digital photographs of the discharge (a) without and (b) with magnetic field (without flow, Canon 600D, exposure time of 1/25 s).

Fig. 3. Schematic diagram of gliding arc with magnetic field

Fig. 4. (a) electrical characteristics of the gliding arc discharge with/without magnetic field; high-speed frames of the gliding arc motion (b) without and (c) with magnetic field (flow rate = 0 L/min; time interval between each gliding arc = 3 ms; exposure time of the camera = 25.2  $\mu$ s)

Fig. 5. The visible emission of a former plasma column in MEGAD (flow rate = 0 L/min).

Fig. 6. (a) electrical characteristics of the gliding arc discharge with/without magnetic field; high-speed frames of the gliding arc motion (b) without and (c) with magnetic field (flow rate = 2 L/min; time interval between each gliding arc = 0.5 ms in (b) and 1.6 ms in (c); exposure time of the camera = 25.2  $\mu$ s)

The gliding arc motions with/without magnetic field show totally different patterns under condition of (2) low flow rate (2 L/min) as well, as seen from Fig. 6. For the MEGAD with magnetic field, a regular cycle of “ignition, elongation and extinguishment” can be clearly observed, indicated from both the electrical characteristics in Fig. 6a and the gliding arc motion behavior in Fig. 6c. The anchor points of plasma column glide down along the electrodes. The averaged cycle period is around 8 ms. In contrast, under conditions without magnetic field, short-circuiting of the plasma column, as further shown in Fig. 7, instead of a complete cycle period happens. Before the real current path is formed, several electron avalanches of Townsend breakdown generate. An example to describe the Townsend breakdown is available in a study by Fridman et al. [32]. Comparing the gliding arc motions

1 in Fig. 6b and 6c, it is obvious that the shape of gliding arc without magnetic field is sharper, which  
2 should be related to the non-uniform distribution of the gas flow field. The sharper shape is apt to cause  
3 a short-circuiting. Around the plasma column, there is a blurred emission signal which can help to  
4 form a new current path as well as the emissions from former plasma gliding arc. Another worth  
5 mentioning phenomenon is that the anchor point of plasma column at the cathode generates a bright  
6 and hot spot, which can be called “cathode spot”, as reported in previous studies [22][33][34]. It has  
7 been proved in a study by Korolev et al [34], that the regime of current sustainment in the near-cathode  
8 regions was corresponded to a normal glow discharge rather than a gliding arc with the discharge  
9 current at a level of 0.2 A. While in the glow regime, the discharge is accompanied by occasional  
10 transitions to a spark. The instability contributes to a micro-explosion of the cathode surface and the  
11 formation of a spark cathode spot. In the GAD without magnetic field, the gas flow is not powerful to  
12 drive the gliding arc so that the cathode spot maintains at a fixed position. This phenomenon will  
13 undoubtedly lead to an accumulation of heat and energy, causing erosion of the electrodes. However,  
14 in the MEGAD with a magnetic field, Lorentz force can produce a synergistic force with the gas flow,  
15 pushing the gliding arc motion along the electrodes without forming a fixed cathode spot. This  
16 characteristic is of great benefit to prolong the use life of the reactor. In order to confirm the electrode  
17 erosion caused by the cathode spot activity, a metalloscope (Axio Scope A1) was used to detect a  
18 section of the cathode surface. As shown in Fig. 8a and 8b, after 30 mins’ discharge, the regular  
19 structure on the anode surface does not change significantly. By contrast, the surface structure of the  
20 cathode has been reshaped and many small craters with diameters of about 50  $\mu\text{m}$  can be observed (see  
21 Fig. 8c), which were caused by the cathode spot.

22

23

24 Fig. 7. A short-circuiting phenomenon in GAD without magnetic field (flow rate = 2 L/min, 39000  
25 frames per second with an exposure time of 25.2  $\mu\text{s}$ ).

26

27

28 Fig. 8. Microscopic photographs of electrode surface before and after 30 mins’ operation (Magnify  
29 200 times)



1  
2  
3  
4  
5  
6  
7  
8  
9  
10  
11  
12  
13  
14  
15  
16  
17  
18  
19  
20  
21  
22  
23  
24  
25  
26  
27  
28  
29

Fig. 9. (a) Electrical characteristics of the gliding arc discharge with/without magnetic field; high-speed frames of the gliding arc motion (b) without and (c) with magnetic field (flow rate = 8 L/min; time interval between each gliding arc = 410  $\mu$ s; exposure time of the camera = 25.2  $\mu$ s)

The physical characteristics of the GAD and MEGAD under the condition of (3) high flow rate (8 L/min) are exhibited in Fig. 9. In this case, for the discharge both with and without magnetic field, the gliding arc ignites, elongates and extinguishes with a regular cycle period of around 0.8 ms. During a cycle, several short-circuitings happen. It can be proposed that, in this case, the drag force from the flow rate, but not the Lorentz force, becomes dominant in propelling the gliding arc moving along the electrodes. Therefore, the gliding arc motion, electrical characteristics and plasma area are almost the same.

Fig. 10. Statistical graph of the cycle periods of the electrical signals under different conditions

Moreover, because only one flat magnet is used in this section for the visibility purpose, it is important to understand how the discharge property is dependent on the magnets or the number of magnets. In this regard, electrical signals of the discharge with no magnet, one magnet, two magnets, at flow rates of 2 and 8 L/min were collected and illustrated in Fig. 10. Each cycle period was recorded 100 times to avoid the errors. As we can see, the addition of magnets significantly increased the cycle period of the electrical signals from around 1 ms to around 7 – 10 ms. The averaged cycle period with two magnets is slightly higher than that with one magnet (9.15 ms and 8.20 ms respectively), indirectly proving that a stronger magnetic field can stretch the gliding arc even more at low flow rates. However, when the flow rate is 8 L/min (see Fig. 10b), the difference between no magnet, one magnet and two magnets become obscure. The average cycle periods are 0.78 ms, 0.79 ms and 0.79 ms respectively, indicating that the magnetic field does not play an observable role in the gliding arc with a higher flow rate (e.g., 8L/min).

1 Obviously, the above results prove that the addition of magnetic field can noticeably optimize the  
2 property of the GAD reactor especially at low gas flow rates, without extra power input. The plasma  
3 reaction volume can be significantly enlarged for chemical reactions. In addition, the “cathode spot”  
4 can move along the electrodes rather than maintaining at a fixed position, which can remarkably  
5 prolong the lifetime of the electrodes. In the GAD without a magnetic field, the pattern of gliding arc  
6 motion is continuous short-circuiting at low flow rate (2 L/min), while the pattern with magnetic field  
7 shows a regular cycle of “ignition, elongation and extinguishment”. It can generate not only a larger  
8 plasma region but also a greater proportion of *non-equilibrium stage*, which is beneficial for a higher  
9 energy efficiency. However, at high flow rate (8 L/min), the addition of magnetic field does not show  
10 remarkable influence on the gliding arc motion and electrical characteristics.

### 11 12 **3.2 CO<sub>2</sub> activation in the MEGAD**

13 In this part, the developed MEGAD is applied to CO<sub>2</sub> dissociation and the effect of the addition  
14 of the magnetic field on the reaction performance is specifically investigated. The feed CO<sub>2</sub> flow rate  
15 is studied as the variable parameter as it can influence significantly both the characteristics of the  
16 discharge and the retention time of the reactant in the plasma area. The effect of flow rate on CO<sub>2</sub>  
17 conversion upon rising flow rate from 1 to 8 L/min is shown in Fig. 10, in reactors with and without  
18 magnetic field. Note that in this section a pair of flat magnets (not a single magnet that used in Section  
19 3.1) were placed both sides of the quartz cover. As can be seen, the addition of magnetic field can  
20 significantly enhance the CO<sub>2</sub> conversion, especially at relatively low flow rates. For example, the CO<sub>2</sub>  
21 conversion is increased by 40.6% from 8.2% to 11.5% when the magnetic field is added. Similar with  
22 our previous study [24][35], in both reactors the CO<sub>2</sub> conversion firstly increases to a maximum value,  
23 from 8.2 % to 11.1 % without magnetic field and from 11.5 % to 12.2 % with the magnetic field, but  
24 then decreases with rising flow rate. The CO<sub>2</sub> conversions at varied flow rates should be directly related  
25 to the gas temperature, retention time and *SEI*. Detailed explanation of this phenomena is available in  
26 our previous works [24][35]. The addition of a magnetic field can enhance the CO<sub>2</sub> conversion,  
27 especially at low flow rates, but the gap of conversions between the GAD and MEGAD become smaller  
28 at high flow rates. For instance, at flow rate of 8 L/min, the CO<sub>2</sub> conversion with/without magnetic  
29 field are almost the same. The variation of CO<sub>2</sub> conversion is consistent with the gliding arc motion

1 and electrical characteristics as above discussed. At a relatively low flow rate, the plasma region in the  
2 MEGAD is much larger than that in GAD, which means a better gas treatment and a longer retention  
3 time. However, at high flow rate, the similar gliding arc motion and electrical characteristics in the two  
4 reactors lead to similar CO<sub>2</sub> conversions. It is interesting to note that the enhancement of the CO<sub>2</sub>  
5 conversion with the addition of magnetic field is realized without the increase of discharge power (or  
6 *SED*), as indicated in Fig. 11. The above results allow us to make a conclusion that the role of magnetic  
7 field in improving the CO<sub>2</sub> conversion performance is more physically, i.e., enlarging the plasma area,  
8 rather than chemically.

9 The energy efficiencies in both reactors are shown in Fig. 12. Obviously, the energy efficiency is  
10 also enhanced with the addition of magnetic field, especially at flow rates of 4 - 6 L/min. The energy  
11 efficiencies in both reactors both increase quickly before 4 L/min due to not only a higher CO<sub>2</sub>  
12 conversion but also an increasing flow rate. Afterwards, the energy efficiency profile without magnetic  
13 field tend to be saturated, while that with magnetic field has a plateau stage (from 4 to 6 L/min) that  
14 followed by a remarkable drop (from 6 to 8 L/min). A maximum energy efficiency of 28.0 % can be  
15 observed at a flow rate of 5 L/min. As mentioned above, the gliding arc motion, electrical  
16 characteristics and CO<sub>2</sub> conversion become more similar between with/without magnetic field at  
17 higher flow rate, which leads to a similar profile of the energy efficiency from 6 to 8 L/min. At last,  
18 the energy efficiency for difference reactors become almost the same at 8 L/min.

19 The above results show that the magnetic field can significantly improve the performance of CO<sub>2</sub>  
20 conversion especially at low flow rates. At an optimal flow rate of 3 L/min, the CO<sub>2</sub> conversion  
21 increases from 11.1 to 12.2 % and energy efficiency increases from 21.7 to 24.3 %, with the addition  
22 of magnetic field. In addition, considering the balance between CO<sub>2</sub> conversion and energy efficiency,  
23 the best results with magnetic field are achieved at a flow rate of 4 L/min, yielding a CO<sub>2</sub> conversion  
24 of 11.2 % and an energy efficiency of 27.9 %.

25  
26  
27 Fig. 10. Variation of CO<sub>2</sub> conversion with increasing flow rate  
28  
29

1 Fig. 11. Variation of *SEI* with increasing flow rate

2  
3 Fig. 12 Variation of energy efficiency with increasing flow rate.

### 4 5 **3.4 Discussion**

6 In Fig. 13, the optimum results of this work are compared with that of other non-thermal plasmas  
7 for CO<sub>2</sub> dissociation in literatures, such as traditional GAD, microwave (MW) plasma, nanosecond-  
8 pulsed (ns-pulse) discharge, corona discharge and dielectric barrier discharge (DBD). In order to fairly  
9 evaluate the industrial applicability, processing capacity is also compared together with the CO<sub>2</sub>  
10 conversion and energy efficiency.

11  
12  
13 Fig. 13 Comparison of the performance of different non-thermal plasmas for CO<sub>2</sub> decomposition:

14 (a) CO<sub>2</sub> conversion; (b) energy efficiency

15  
16 Obviously, microwave plasma presents remarkable results, e.g., 30 % CO<sub>2</sub> conversion and 40 %  
17 energy efficiency at a flow rate of 5000 mL/min as reported by Van Rooij et al. [36] and 42 % CO<sub>2</sub>  
18 conversion and 17.5 % energy efficiency at a flow rate of 2000 mL/min as reported by Chen et al. [37].  
19 But it should be mentioned that the high conversion and efficiency of MW plasma were obtained only  
20 in low pressure systems (e.g., 150 mbar [36] and 10 Torr [37]) and the energy consumed in the vacuum  
21 system was not taken into account. Obviously, it is costly to maintain a negative pressure and thus  
22 undesirable for industrial applicability. As clearly shown, DBD [38][39][40][41][42][43] can exhibit  
23 an impressive CO<sub>2</sub> conversion, but the energy efficiency (2.0 ~ 16.8 %) is unattractive. Meanwhile,  
24 most of the reported works in DBD were performed with the presence of catalysts, such as CaTiO<sub>3</sub>  
25 [39], ZrO<sub>2</sub> [42], BaTiO<sub>3</sub> and TiO<sub>2</sub> [43]. However, the preparation of catalyst is time-consuming and  
26 costly. Furthermore, the catalyst deactivation is still a severe problem to be solved. GAD exhibits a  
27 similar CO<sub>2</sub> conversion with that of ns-pulse discharge [44], corona discharge [45] and some of DBDs,  
28 but have a notable performance in energy efficiency. In addition, the significantly higher processing  
29 capacity is promising for the industrial applicability.

1 In this work, a magnetic field was used to enlarge the plasma area, and (1) a 12.2% CO<sub>2</sub>  
2 conversion and 24.3% energy efficiency can be reached at a flow rate of 3000 mL/min; (2) a 11.2%  
3 CO<sub>2</sub> conversion and 27.9% energy efficiency can be reached in 4000 mL/min. The energy efficiency  
4 and processing capacity of the MEGAD are indeed promising and better than other that of other plasma  
5 types at atmospheric pressure. There is still room for GAD to improve. The limited fraction of gas  
6 treated and the relatively high gas temperature are still the major limiting factors [8][46]. Therefore,  
7 cooling the plasma reaction area and further increasing the plasma area by optimizing the reactor  
8 configuration are expected to further enhance the CO<sub>2</sub> dissociation performance.

#### 9 10 **4. Conclusion**

11 In this work, a novel magnetically enhanced gliding arc discharge (MEGAD) reactor was  
12 developed and investigated for CO<sub>2</sub> decomposition. The gliding arc motion behavior, electrical  
13 characteristics and CO<sub>2</sub> decomposition performance of the MEGAD reactor are investigated with  
14 specific attention on the role of magnetic field.

15 Interestingly, a large 70 mm length plasma area can be formed in the MEGAD even without gas  
16 injected, while in a GAD without magnetic field, a highly bright and stable gliding arc is maintained  
17 in the narrowest gap between two electrodes and no 3D plasma area is formed for chemical reaction.  
18 At a moderate flow rate of 2 L/min, a short-circuiting pattern is formed in the GAD without magnetic  
19 field. Several electron avalanches of Townsend breakdown were observed during a new short-  
20 circuiting. On the contrary, the MEGAD shows a regular motion cycle of “ignition – elongation –  
21 extinguishment”, forming a significant larger plasma area for chemical reaction. However, when  
22 further increasing the flow rate to 8 L/min, the motion behavior and the electrical characteristics of the  
23 GAD and MEGAD show no significant difference.

24 The magnetic field can noticeably enhance the performance of a GAD reactor by producing a  
25 significantly larger plasma region for chemical reactions especially at low gas flow rates, due to the  
26 synergistic effect of Lorentz force and gas flow. In addition, the “cathode spot” in the MEGAD is not  
27 anchored at a fixed position, alleviating the erosion problem of electrodes at high temperatures and  
28 remarkably prolonging the use life of the reactor.

29 The addition of magnetic field can significantly improve the performance of CO<sub>2</sub> conversion

1 especially at low flow rates. At a flow rate of 1 L/min, the CO<sub>2</sub> conversion is increased by 40.6 %  
2 (from 8.2 to 11.5 %) and the energy efficiency is increased 35.6 % (from 5.8 to 8.0 %). However, the  
3 CO<sub>2</sub> conversion gap and energy efficiency gap between the GAD and MEGAD become smaller at  
4 higher flow rates, which corresponds to the gliding arc motion and electrical characteristics. The results  
5 indicate that the role of magnetic field in improving the CO<sub>2</sub> conversion performance is more physical,  
6 i.e., enlarging the plasma area, rather than chemical conversion.

7 The optimal CO<sub>2</sub> dissociation performance is achieved with the presence of a magnetic field, i.e.,  
8 12.2% CO<sub>2</sub> conversion and 24.3% energy efficiency at 3000 mL/min; 11.2% CO<sub>2</sub> conversion and 27.9%  
9 energy efficiency at 4000 mL/min. Compared to other commonly used non-thermal atmosphere  
10 pressure plasma reactors, the MEGAD shows a better energy efficiency and remarkably higher  
11 processing capacity.

12

### 13 **Acknowledgements**

14 This work is supported by the National Natural Science Foundation of China (No. 51706204 and No.  
15 51576174) and the China Postdoctoral Science Foundation (No. 2018M630673).

## 1 Reference

- 2 [1] C. Quéré *et al.*, “Global Carbon Budget 2018,” *Earth Syst. Sci. Data*, 2018.
- 3 [2] P. Köhler, J. F. Abrams, C. Völker, J. Hauck, and D. A. Wolf-Gladrow, “Geoengineering impact of open  
4 ocean dissolution of olivine on atmospheric CO<sub>2</sub>, surface ocean pH and marine biology,” *Environ. Res.  
5 Lett.*, 2013.
- 6 [3] X. Zhang, J. L. Fan, and Y. M. Wei, “Technology roadmap study on carbon capture, utilization and  
7 storage in China,” *Energy Policy*, 2013.
- 8 [4] B. Smit, A.-H. A. Park, and G. Gadikota, “The Grand Challenges in Carbon Capture, Utilization, and  
9 Storage,” *Front. Energy Res.*, vol. 2, no. November, pp. 2013–2015, 2014.
- 10 [5] D. S. Laitar, P. Müller, and J. P. Sadighi, “Efficient homogeneous catalysis in the reduction of CO<sub>2</sub> to  
11 CO,” *J. Am. Chem. Soc.*, 2005.
- 12 [6] J. L. Liu, H. W. Park, W. J. Chung, and D. W. Park, “High-Efficient Conversion of CO<sub>2</sub> in AC-Pulsed  
13 Tornado Gliding Arc Plasma,” *Plasma Chem. Plasma Process.*, vol. 36, no. 2, pp. 437–449, 2016.
- 14 [7] C. Nigara, Yutaka, Bernard, “Production of CO by direct thermal splitting of CO<sub>2</sub> at high temperature,”  
15 *The Chemical Society of Japan*, vol. 59. pp. 1997–2002, 1986.
- 16 [8] S. R. Sun, H. X. Wang, D. H. Mei, X. Tu, and A. Bogaerts, “CO<sub>2</sub> conversion in a gliding arc plasma:  
17 Performance improvement based on chemical reaction modeling,” *J. CO<sub>2</sub> Util.*, vol. 17, pp. 220–234,  
18 2017.
- 19 [9] H. Zhang *et al.*, “Steam reforming of toluene and naphthalene as tar surrogate in a gliding arc discharge  
20 reactor,” *J. Hazard. Mater.*, vol. 369, no. January, pp. 244–253, 2019.
- 21 [10] H. Zhang, F. Zhu, X. Li, K. Cen, C. Du, and X. Tu, “Enhanced hydrogen production by methanol  
22 decomposition using a novel rotating gliding arc discharge plasma,” *RSC Adv.*, vol. 6, no. 16, pp. 12770–  
23 12781, 2016.
- 24 [11] H. Zhang, X. Li, F. Zhu, K. Cen, C. Du, and X. Tu, “Plasma assisted dry reforming of methanol for clean  
25 syngas production and high-efficiency CO<sub>2</sub> conversion,” *Chem. Eng. J.*, vol. 310, pp. 114–119, 2017.
- 26 [12] H. Zhang *et al.*, “Plasma activation of methane for hydrogen production in a N<sub>2</sub> rotating gliding arc  
27 warm plasma: A chemical kinetics study,” *Chem. Eng. J.*, vol. 345, no. September 2017, pp. 67–78, 2018.
- 28 [13] R. Snoeckx and A. Bogaerts, “Plasma technology—a novel solution for CO<sub>2</sub> conversion?,” *Chemical  
29 Society Reviews*. 2017.
- 30 [14] R. Snoeckx, S. Heijckers, K. Van Wesenbeeck, S. Lenaerts, and A. Bogaerts, “CO<sub>2</sub> conversion in a dielectric  
31 barrier discharge plasma: N<sub>2</sub> in the mix as a helping hand or problematic impurity?,” *Energy Environ.  
32 Sci.*, vol. 9, no. 3, pp. 999–1011, 2016.
- 33 [15] A. Fridman, S. Nester, L. A. Kennedy, A. Saveliev, and O. Mutaf-Yardimci, “Gliding arc gas discharge,”  
34 *Prog. Energy Combust. Sci.*, 1999.
- 35 [16] W. Wang, A. Berthelot, S. Kolev, X. Tu, and A. Bogaerts, “CO<sub>2</sub> conversion in a gliding arc plasma: 1D  
36 cylindrical discharge model,” *Plasma Sources Sci. Technol.*, vol. 25, no. 6, p. 65012, 2016.
- 37 [17] M. Ramakers, G. Trenchev, S. Heijckers, W. Wang, and A. Bogaerts, “Gliding Arc Plasmatron: Providing an  
38 Alternative Method for Carbon Dioxide Conversion,” *ChemSusChem*, vol. 10, no. 12, pp. 2642–2652,  
39 2017.
- 40 [18] A. Berthelot and A. Bogaerts, “Modeling of CO<sub>2</sub> Splitting in a Microwave Plasma: How to Improve the  
41 Conversion and Energy Efficiency,” *J. Phys. Chem. C*, vol. 121, no. 15, pp. 8236–8251, 2017.
- 42 [19] H. Zhang, F. Zhu, X. Tu, Z. Bo, K. Cen, and X. Li, “Characteristics of Atmospheric Pressure Rotating Gliding  
43 Arc Plasmas,” *Plasma Sci. Technol.*, vol. 18, no. 5, pp. 473–477, 2016.
- 44 [20] S. P. Gangoli, A. F. Gutsol, and A. A. Fridman, “A non-equilibrium plasma source: Magnetically stabilized

- 1 gliding arc discharge: I. Design and diagnostics," *Plasma Sources Sci. Technol.*, vol. 19, no. 6, 2010.
- 2 [21] T. Kozák and A. Bogaerts, "Splitting of CO<sub>2</sub> by vibrational excitation in non-equilibrium plasmas: A  
3 reaction kinetics model," *Plasma Sources Sci. Technol.*, 2014.
- 4 [22] Y. D. Korolev, O. B. Frants, N. V. Landl, A. V. Bolotov, and V. O. Nekhoroshev, "Features of a near-  
5 cathode region in a gliding arc discharge in air flow," *Plasma Sources Sci. Technol.*, vol. 23, no. 5, 2014.
- 6 [23] H. Zhang, X. D. Li, Y. Q. Zhang, T. Chen, J. H. Yan, and C. M. Du, "Rotating gliding arc codriven by  
7 magnetic field and tangential flow," *IEEE Trans. Plasma Sci.*, vol. 40, no. 12, pp. 3493–3498, 2012.
- 8 [24] H. Zhang, L. Li, X. Li, W. Wang, J. Yan, and X. Tu, "Warm plasma activation of CO<sub>2</sub> in a rotating gliding arc  
9 discharge reactor," *J. CO<sub>2</sub> Util.*, vol. 27, no. March, pp. 472–479, 2018.
- 10 [25] N. Balcon, N. Benard, P. Braud, A. Mizuno, G. Touchard, and E. Moreau, "Prospects of airflow control by a  
11 gliding arc in a static magnetic field," *J. Phys. D: Appl. Phys.*, vol. 41, no. 20, 2008.
- 12 [26] L. Hui, M. Qing, L. Lincun, and X. Weidong, "Determination of the Velocity of a Magnetic-Field Driven  
13 Gliding Arc by Using a Photo-Multiplier," *Plasma Sci. Technol.*, vol. 6, no. 6, pp. 2593–2595, 2006.
- 14 [27] A. Indarto, D. R. Yang, J. W. Choi, H. Lee, and H. K. Song, "Gliding arc plasma processing of  
15 CO<sub>2</sub> conversion," *J. Hazard. Mater.*, vol. 146, no. 1–2, pp. 309–315, 2007.
- 16 [28] S. C. Kim and Y. N. Chun, "Development of a gliding arc plasma reactor for CO<sub>2</sub> destruction," *Environ.  
17 Technol. (United Kingdom)*, vol. 35, no. 23, pp. 2940–2946, 2014.
- 18 [29] S. C. Kim, M. S. Lim, and Y. N. Chun, "Reduction characteristics of carbon dioxide using a plasmatron,"  
19 *Plasma Chem. Plasma Process.*, vol. 34, no. 1, pp. 125–143, 2014.
- 20 [30] O. Mutaf-Yardimci, A. V. Saveliev, A. A. Fridman, and L. A. Kennedy, "Thermal and nonthermal regimes of  
21 gliding arc discharge in air flow," *J. Appl. Phys.*, vol. 87, no. 4, pp. 1632–1641, 2000.
- 22 [31] Z. W. Sun *et al.*, "Optical diagnostics of a gliding arc," *Opt. Express*, vol. 21, no. 5, p. 6028, 2013.
- 23 [32] A. Fridman, A. Chirokov, and A. Gutsol, "Non-thermal atmospheric pressure discharges," *J. Phys. D:  
24 Appl. Phys.*, vol. 38, no. 2, 2005.
- 25 [33] Y. D. Korolev, O. B. Frants, N. V. Landl, V. G. Geyman, and I. B. Matveev, "Glow-to-spark transitions in a  
26 plasma system for ignition and combustion control," *IEEE Trans. Plasma Sci.*, vol. 35, no. 6 PART 1, pp.  
27 1651–1657, 2007.
- 28 [34] Y. D. Korolev, O. B. Frants, V. G. Geyman, N. V. Landl, and V. S. Kasyanov, "Low-current 'gliding Arc'  
29 in an air flow," *IEEE Trans. Plasma Sci.*, vol. 39, no. 12 PART 1, pp. 3319–3325, 2011.
- 30 [35] L. Li *et al.*, "Plasma-assisted CO<sub>2</sub> conversion in a gliding arc discharge: Improving performance by  
31 optimizing the reactor design," *J. CO<sub>2</sub> Util.*, vol. 29, no. October 2018, pp. 296–303, 2019.
- 32 [36] G. J. Van Rooij *et al.*, "Taming microwave plasma to beat thermodynamics in CO<sub>2</sub> dissociation," *Faraday  
33 Discuss.*, vol. 183, pp. 233–248, 2015.
- 34 [37] G. Chen, V. Georgieva, T. Godfroid, R. Snyders, and M. P. Delplancke-Ogletree, "Plasma assisted catalytic  
35 decomposition of CO<sub>2</sub>," *Appl. Catal. B Environ.*, vol. 190, pp. 115–124, 2016.
- 36 [38] R. Aerts, W. Somers, and A. Bogaerts, "Carbon Dioxide Splitting in a Dielectric Barrier Discharge Plasma:  
37 A Combined Experimental and Computational Study," *ChemSusChem*, vol. 8, no. 4, pp. 702–716, 2015.
- 38 [39] Q. Yu, M. Kong, T. Liu, J. Fei, and X. Zheng, "Characteristics of the decomposition of CO<sub>2</sub> in a dielectric  
39 packed-bed plasma reactor," *Plasma Chem. Plasma Process.*, vol. 32, no. 1, pp. 153–163, 2012.
- 40 [40] I. Belov, S. Paulussen, and A. Bogaerts, "Appearance of a conductive carbonaceous coating in a  
41 CO<sub>2</sub> dielectric barrier discharge and its influence on the electrical properties and the conversion  
42 efficiency," *Plasma Sources Sci. Technol.*, 2016.
- 43 [41] A. Ozkan *et al.*, "The influence of power and frequency on the filamentary behavior of a flowing DBD -  
44 Application to the splitting of CO<sub>2</sub>," *Plasma Sources Sci. Technol.*, vol. 25, no. 2, 2016.



- 1 [42] K. Van Laer and A. Bogaerts, "Improving the Conversion and Energy Efficiency of Carbon Dioxide  
2 Splitting in a Zirconia-Packed Dielectric Barrier Discharge Reactor," *Energy Technol.*, vol. 3, no. 10, pp.  
3 1038–1044, 2015.
- 4 [43] D. Mei, X. Zhu, C. Wu, B. Ashford, P. T. Williams, and X. Tu, "Plasma-photocatalytic conversion of CO<sub>2</sub> at  
5 low temperatures: Understanding the synergistic effect of plasma-catalysis," *Appl. Catal. B Environ.*, vol.  
6 182, pp. 525–532, 2016.
- 7 [44] M. S. Bak, S. K. Im, and M. Cappelli, "Nanosecond-pulsed discharge plasma splitting of carbon dioxide,"  
8 *IEEE Trans. Plasma Sci.*, vol. 43, no. 4, pp. 1002–1007, 2015.
- 9 [45] W. Xu, M. W. Li, G. H. Xu, and Y. L. Tian, "Decomposition of CO<sub>2</sub> using DC corona discharge at  
10 atmospheric pressure," *Japanese J. Appl. Physics, Part 1 Regul. Pap. Short Notes Rev. Pap.*, vol. 43, no.  
11 12, pp. 8310–8311, 2004.
- 12 [46] R. Snoeckx and A. Bogaerts, "Plasma technology—a novel solution for CO<sub>2</sub> conversion?," *Chem. Soc.  
13 Rev.*, vol. 46, no. 19, pp. 5805–5863, 2017.
- 14  
15